

Mechanics modelling of fern cavitation catapult

Jingtian Kang, Kai Li, Huifeng Tan, Changguo Wang, and Shengqiang Cai

Citation: *Journal of Applied Physics* **122**, 225105 (2017);

View online: <https://doi.org/10.1063/1.5009747>

View Table of Contents: <http://aip.scitation.org/toc/jap/122/22>

Published by the [American Institute of Physics](#)

Scilight

Sharp, quick summaries **illuminating**
the latest physics research

Sign up for **FREE!**



Mechanics modelling of fern cavitation catapult

Jingtian Kang,^{1,2} Kai Li,^{1,3} Huifeng Tan,² Changguo Wang,^{2,a)} and Shengqiang Cai^{1,a)}

¹*Department of Mechanical and Aerospace Engineering, University of California, San Diego, La Jolla, California 92093, USA*

²*Center for Composite Materials, Harbin Institute of Technology, Harbin 150001, People's Republic of China*

³*Department of Civil Engineering, Anhui Jianzhu University, Hefei, Anhui 230601, People's Republic of China*

(Received 19 October 2017; accepted 24 November 2017; published online 12 December 2017)

Cavitation is often regarded as a failure mode in soft materials. An intriguing phenomenon has been recently discovered that fern sporangium can take advantage of drying-induced cavitation instability in annulus cells to disperse spores at an extraordinarily high acceleration. Briefly, the decrease of environmental humidity causes continuous bending of the sporangium and growth of cavities inside the annulus cells, with the elastic energy accumulated in sporangium walls. When the humidity is lower than a critical value, the cavities suddenly expand dramatically inside the cells, causing a quick release of the elastic energy stored in the annular structure. As a result, like a catapult, the sporangium snaps back and ejects the seeds at a high speed. Motivated by the observation, in this article, we study cavitation instability in a similar structure as the sporangium. To simplify the problem, in our model, the mechanics of cells in the sporangium are described by the polymer gel model, while the sporangium wall is modelled as a hyperelastic material. When the environmental humidity is lower than a critical value, through energetic analyses, we can predict the cavitation catapult phenomenon using the model. We hope that our study in this article can provide useful insights into the bio-inspired design of structures which can take advantage of cavitation instability in soft materials. *Published by AIP Publishing.* <https://doi.org/10.1063/1.5009747>

I. INTRODUCTION

Plants can move in response to a variety of stimuli such as light, temperature, humidity, or even a gentle mechanical touch.^{1,2} Although the movement of plants is typically much slower than animals due to the lack of muscles, in certain scenarios, plants can also generate very fast motions through elastic instability, fracture, or cavitation. For instance, the fast closure of snap traps of the Venus flytrap results from snap-buckling instability.^{3–5} As another example, cavitation in cells has also been used by other plants like *Curvularia*, *Zygophalia jamaicensis*, *Memnoniella subsimplex*, and fern sporangium to generate fast motion.⁶

Cavitation in soft solids such as rubber, gels, and some biological tissues has been commonly recognized as one failure mechanism.^{7–12} Pioneering work done by Gent has shown that when a soft elastomer is subjected to hydrostatic tension approaching 2.5 times of its shear modulus, small cavities inside the elastomer may expand significantly and cause the failure of the material.^{13–17} Reflection of the blast-induced compressive wave in the brain can also generate a large hydrostatic tension which may consequently result in cavitation, as well as damages to the brain tissue.¹⁸ Recently, we have found that drying can also cause cavitation instability in a swollen gel with external constraints.^{19,20} Since cavitation in soft solids often induces a large deformation or even damage to the material,^{21–25} according to our knowledge, few engineering structures have ever been fabricated to make use of cavitation to realize novel functions.^{26–28}

Some recent experimental studies have uncovered very interesting phenomena that fern sporangium can eject spores with an initial speed of up to 10 m/s and an acceleration of 106 g using the cavitation catapult mechanism.²⁹ The term, cavitation catapult, is a vivid analogy that the fern sporangium exhibits fast closure motion to propel the spores like a catapult by cavitation instability as shown in Fig. 1. Briefly, triggered by the decrease of environmental humidity, the entire spore dispersal process of fern sporangium can be roughly divided into three stages, i.e., opening, fast bouncing back, and closing.³⁰ During the opening stage, a sporangium opens slowly and stores bending energy in the annulus wall, accompanied by the shrinkage of cells and loss of water, as shown in Fig. 1(b). The fast bouncing back stage is caused by the sudden and dramatic expansion of cavities inside cells as shown in Fig. 1(c). Finally, the closing stage makes the entire structure recover its original configuration. The sudden and dramatic growth of cavities in the annulus cells plays a vital role in dispensing the spores to a long distance.

According to our knowledge, though cavitation instabilities have been adopted by several different plants for fast motion such as the cavitation catapult in fern sporangium discussed above, the underlying mechanism has not been carefully studied, and a mechanics model of such a mechanism does not exist. In this paper, we develop a mechanics model of the cavitation catapult mechanism of fern sporangium. The paper is organized as follows: in Sec. II, we propose a computational method to investigate cavitation instability in a partially constrained gel subject to traction and change of chemical potential of the solvent. In Sec. III, we study the cavitation catapult mechanism in the sporangium by using the computational method developed in Sec. II. To simplify the

^{a)}Authors to whom correspondence should be addressed: shqcai@ucsd.edu and wangcg@hit.edu.cn.

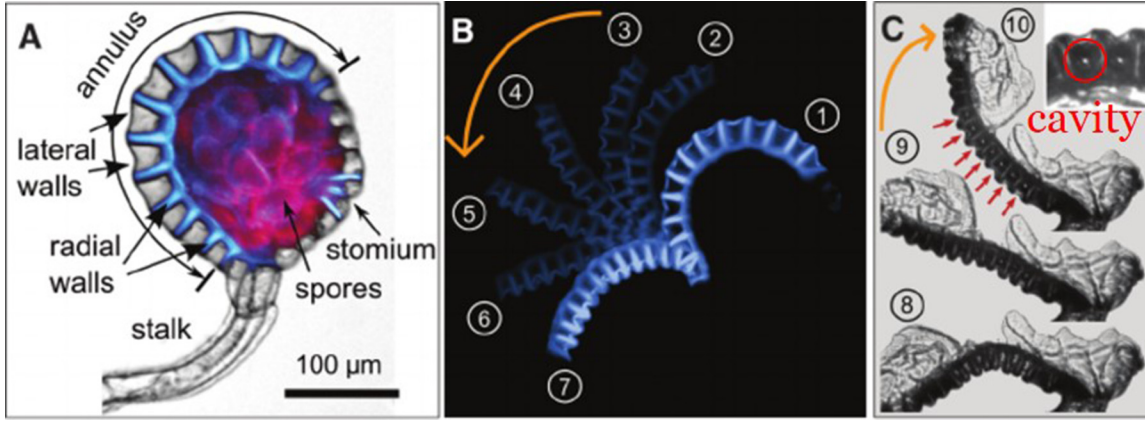


FIG. 1. Cavitation catapult phenomenon of a fern sporangium (with the permission of the AAAS).²⁹ (a) The structure of the sporangium of *Polypodium aur-eum*. (b) A decrease of environmental humidity makes the annulus open gradually. (c) Sudden snap back of the annulus due to the appearance of cavities within annulus cells.

problem, we use a gel model to describe the environmentally responsive mechanical behaviors of cells in the sporangium. We conduct finite element simulation to calculate the free energy of the system by controlling the volumes of the cavities. By further assuming that the system always stays in a deformed configuration with the lowest free energy, we successfully predict discontinuous expansion of cavities in the cell of the sporangium, as well as curvature change of the annulus wall. We hope that our study in this article can provide useful insights into the bio-inspired design of structures taking advantages of cavitation instability in soft materials.

II. MECHANICS MODEL OF CAVITATION INSTABILITY IN A CELL

A. Constitutive model of a polymer gel

To develop a mechanics model of the cavitation catapult mechanism of fern sporangium, we will adopt the constitutive model of a polymer gel to describe the environmentally responsive mechanical behaviors of cells as shown in Fig. 1, by considering the following reasons: (1) mechanical behaviors of an individual cell are too complex to model precisely, which is also beyond the scope of the current article; (2) it has been well recognized that the mechanical behaviors of the cell and polymer gel have several common features.^{31,32} For example, both the cell and polymer gel can swell by absorbing water when the environmental humidity is high, and shrink when the humidity is low; both the cell and polymer gel can be viewed as incompressible soft solids if the total amount of the solvent inside remains unchanged. Next, we will briefly review the constitutive model of a polymer gel, which has been previously developed by us and others.^{33,34}

Following previous studies on the constitutive modelling of a polymer gel,³³ we regard a stress-free and dry gel as the reference state. The gel can deform when stress is applied onto it or when the chemical potential of the solvent in the environment changes. Deformation gradient of the gel can be given by

$$F_{iK} = \frac{\partial x_i(\mathbf{X})}{\partial X_K}, \quad (1)$$

where X_K and x_i are the coordinates of the same material point in the reference state and current state, respectively. The nominal stress s_{iK} and deformation gradient is a work-conjugate pair, and the chemical potential of the solvent in the gel μ and its concentration C is another work-conjugate pair, namely,

$$s_{iK} = \frac{\partial W(F_{iK}, C)}{\partial F_{iK}} \quad \text{and} \quad \mu = \frac{\partial W(F_{iK}, C)}{\partial C}, \quad (2)$$

where W is the free energy density of the gel and C is defined as the number of solvent molecules per unit volume of the gel in the reference state.

Based on the Flory–Rehner model,³⁵ the free energy density of a polymer gel can be decomposed into two parts: elastic energy of the stretching polymer network and mixing free energy between the polymer and solvent. Explicitly, the free energy density of a gel can be given by

$$W(F_{iK}, C) = \frac{1}{2}NkT(F_{iK}F_{iK} - 3 - 2\log J) - \frac{kT}{\Omega} \left[\Omega C \log \left(\frac{\Omega C + 1}{\Omega C} \right) + \frac{\chi}{\Omega C + 1} \right], \quad (3)$$

where Ω is the volume per solvent molecule, N is the number of polymer chains per volume in the reference state, χ is a dimensionless parameter measuring the energy of mixing, kT is the absolute temperature in the unit of energy, and $J = \det F_{iK}$ is the determinant of the deformation gradient.

Following previous work,³³ we adopt molecular incompressible assumption which can be written as $J = 1 + \Omega C$. To integrate the constitutive model into finite element modelling, it is convenient to change the variable C to chemical potential μ by a Legendre transformation

$$\hat{W}(F_{iK}, \mu) = W(F_{iK}, C) - \mu C. \quad (4)$$

Consequently, we can obtain

$$\hat{W}(F_{iK}, \mu) = \frac{1}{2}NkT(F_{iK}F_{iK} - 3 - 2\log J) - \frac{kT}{\Omega} \left[(J - 1) \log \left(\frac{J}{J - 1} \right) + \frac{\chi}{J} \right] - \frac{\mu}{\Omega}(J - 1). \quad (5)$$

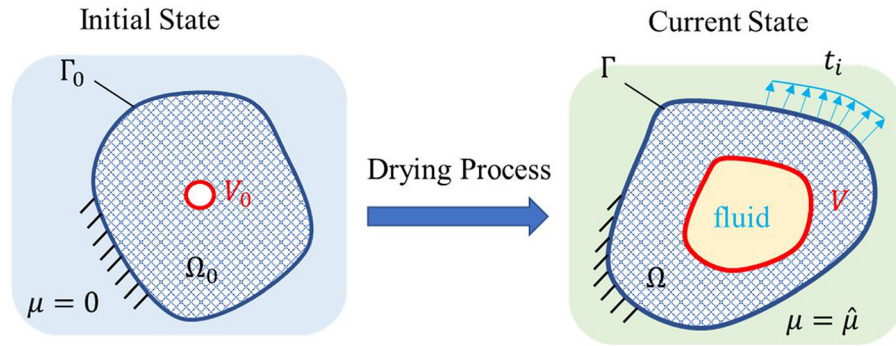


FIG. 2. The schematic of our computational method for analyzing cavitation instability in a gel during the drying process with constraint and applied forces. In the initial state, a small cavity is introduced into a swollen gel with mechanical constraints. With the change of the chemical potential of the solvent and application of traction on the surface of the gel, the cavity may expand and deform. To control the volume of the cavity, we use an incompressible fluid to occupy the space of the cavity as a technical approach. The volume of the fluid can only be changed by changing its temperature, but not by applying stress. Therefore, in the simulation, we can precisely control the volume of the cavity by varying the temperature of the fluid with the assigned thermal expansion coefficient.

Equation (2) can then be rewritten as: $s_{iK} = \frac{\partial \hat{W}(F_{iK}, \mu)}{\partial F_{iK}}$. If the solvent is water, we can simply link the chemical potential of the solvent to the environmental humidity by $\mu = kT \log RH$, where RH is the relative humidity of the environment.

In the current study, we conduct a quasi-static analysis and only focus on the equilibrium state of the structure. Therefore, the chemical potential in Eq. (5) is set to be homogenous everywhere in the gel. We implement Eq. (5) into the commercial software ABAQUS³⁶ as a constitutive model of the gel using the user-defined subroutine (UHYPER) proposed by Hong *et al.*³⁷

B. Computational method of cavitation instability in a constrained gel

As shown in Fig. 1 and previous discussions, drying of a constrained cell in the fern sporangium can trigger cavitation instability. During the drying process, the environmental humidity decreases, so the cell loses water and intends to shrink. Due to the existence of mechanical constraints of the annulus walls, tensile stress can be generated in the cell and a small cavity/defect expands.

Cavity expansion in a cell can be either continuous or discontinuous. To model both continuous and discontinuous cavitation expansion in a cell, we develop a computational modelling method in a constrained gel as shown in Fig. 2. In the initial state, a tiny spherical cavity with volume V_0 is introduced into a swollen gel with homogeneous chemical potential of the solvent μ . Displacement of the gel surface may be completely or partially fixed. When the chemical potential of the solvent changes, and tractions are applied onto the gel surface, the cavity deforms and expands. To model the cavity expansion using the finite element method, we control the volume of the cavity by filling the cavity with an incompressible fluid, which has been used in our previous study.³⁸ The volume of the fluid cannot be changed by changing the pressure applied onto it. Instead, we can change the volume of the fluid with the assigned thermal expansion coefficient by tuning its temperature. It is noted that the thermal expansion of the liquid inside the cavity is used to precisely control the cavity volume in the FEM simulation, which does not correspond to any real physical process. The

entire cavitating process is assumed to be in the isothermal condition. In the simulation, the linear thermal expansion of the liquid is adopted.

Specifically, modelling cavitation in a constrained gel caused by drying is composed of two main steps. First, we compute the deformation of the gel caused by the change of the chemical potential of the solvent and the application of tractions, by fixing the volume of a cavity. Subsequently, we change the volume of a cavity gradually by changing the thermal expansion of the fluid filled in it. The equilibrium configuration of the entire structure can be calculated by finite element simulation. As shown in some previous studies,^{20,25} surface tension can play an important role in cavitation. To take account of the effects of surface tension, we calculate the free energy of the system as

$$F = \Phi + A\gamma, \quad (6)$$

where Φ is the free energy of the structure obtained from finite element simulation, A is the surface area of the cavity, and γ is the surface tension. As a result, the free energy of the structure can be obtained as a function of the volume of the cavity. By assuming the structure always stays in the state with minimized free energy, we can determine the volume of the cavity in the gel with known chemical potential of the solvent and applied tractions.

In the analysis described above, we neglect the effects of surface energy on the deformation of the structure. The assumption that elastic and surface energies are independent is not strictly correct, as the shape of the cavity can change to minimize the combined energy in Eq. (6). However, it is fairly complex to solve the coupled elastocapillary problem via FEM simulation, as shown in recent studies.^{25,39–41} While this simplifying assumption undoubtedly leads to errors in the calculated energy landscape, especially for small cavities, we believe it does not change the qualitative behavior. Further, as we will show later, this simple treatment enables us to capture the main features of the cavitation catapult phenomenon.

C. Validation of the computational method

To validate the computational method proposed above, we compare the numerical results with the analytical results

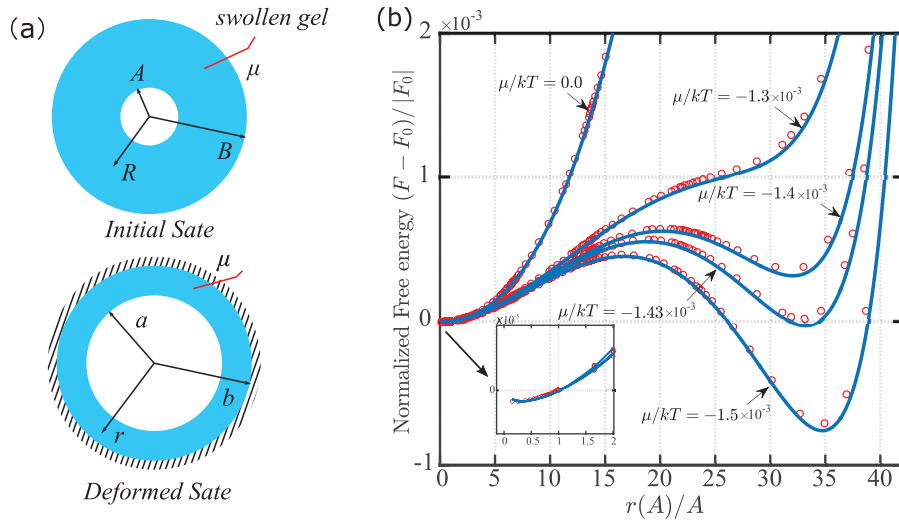


FIG. 3. Validation of our computational model by comparing the analytical solution of cavitation in a swollen spherical gel under external constraint with the simulation results. The open circles are the simulation results and the solid lines are the analytical results from our previous study.²⁰ The surface energy density is $\gamma/(NkTA) = 20$ and F_0 is the free energy of the system when the volume of the cavity is the same as its initial stage.

of drying-induced cavitation in a constrained spherical gel obtained in a previous paper.²⁰ A free swelling spherical gel with an initially introduced infinitesimal cavity is constrained by its external boundary. With the decrease of the chemical potential of the solvent, we can calculate the free energy of the gel as a function of cavity size, both analytically and numerically. The material parameters shown in Eq. (3) are set to be $N\Omega = 10^{-3}$ and $\chi = 0.2$. In the finite element simulation, we use 1200 CAX4H elements for the gel and embed 40 F2D2 fluid elements on the surface of the cavity for simulating the fluid filled in the cavity. We assign the linear thermal expansion coefficient and temperature change to the fluid elements to control the volume of the fluid filled inside the cavity in the simulation. Figure 3 shows the comparison between the free energy of the constrained spherical gel as a function of cavity size obtained from finite element simulation and analytical formulation. The agreement of the results as shown in Fig. 3 validates the simulation method proposed above.

III. RESULTS AND DISCUSSIONS

A. Cavitation instability of a partially constrained gel

In this section, we first study cavitation instability in a partially constrained gel as shown in Fig. 4. We consider a free-standing gel in a dry state as the reference state as shown in Fig. 4(a). The width and height of the rectangular gel are W and H , respectively, with an aspect ratio $W/H = 0.5$. Without losing generality, we assume the deformation of the gel is in

the plane-strain condition. A tiny circular cavity is introduced in the center of the gel. The radius of the cavity is set to be 2% of its width. In the initial state, as shown in Fig. 4(b), the dry gel swells freely with the swelling ratio λ_0 and the chemical potential of the solvent in the gel becomes zero. Consequently, the width and height of the gel become $\lambda_0 W$ and $\lambda_0 H$, respectively, and the radius of the cavity becomes $\lambda_0 A$. During the drying process, as shown in Fig. 4(c), the left, right, and bottom surfaces of the free-swollen gel are constrained by rigid walls, while its top surface is maintained traction-free, and the chemical potential of the solvent in the environment decreases. To stay in a chemo-mechanical equilibrium state, the gel loses the solvent and intends to shrink, resulting in the expansion of the cavity as shown in Fig. 4(c). Because of the influence of constraints, the shape of the cavity deviates from its initial circular shape during expansion.

The constitutive model of the gel is given by Eq. (5). In the simulation, the material parameters of the gel are set to be $N\Omega = 10^{-3}$ and $\chi = 0.2$, which are representative values for most hydrogels. We have also verified that varying these two values within a reasonable range can lead to some quantitative, but not qualitative, change of our results. Based on Eq. (5) and our previous work,²⁰ it is easy to show that the swelling ratio λ_0 of a free-standing gel can be determined by solving the following nonlinear algebra equation:

$$Nv \left(\frac{1}{\lambda_0} - \frac{1}{\lambda_0^3} \right) + \log \left(1 - \frac{1}{\lambda_0^3} \right) + \frac{1}{\lambda_0^3} + \frac{\chi}{\lambda_0^6} = 0. \quad (7)$$

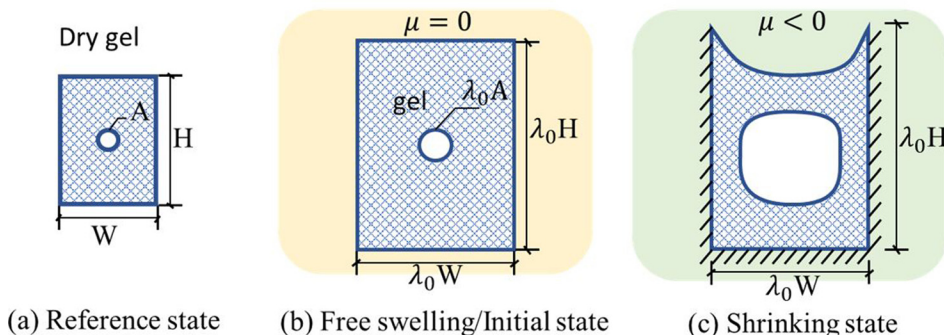


FIG. 4. The schematic of the numerical simulation of a partially constrained gel. (a) Dry hydrogel with a small cavity inside is regarded as the reference state. (b) Free swelling state of the hydrogel with the chemical potential of water $\mu = 0$. (c) The swollen hydrogel is partially constrained. Decrease of the chemical potential of the water in the environment may result in continuous or discontinuous expansion of the cavity.

$\lambda_0 = 3.215$ is the only solution for the above equation. In the simulation, there are 1022 CPE4H elements for the gel. The cavity is filled with an incompressible fluid with 26 F2D2 elements on the cavitation surface. The number of elements is determined through a mesh convergence check. The boundary conditions are the same as that illustrated in Fig. 4(c). During the numerical simulation process, in the first step, we decrease the chemical potential of the solvent in the gel from zero to an aimed negative value; in the second step, we increase the volume of the incompressible fluid through thermal expansion while keeping the chemical potential of the solvent unchanged. As a result, we can obtain the equilibrium configurations of the gel for a fixed chemical potential of the solvent and different volumes of the cavity from finite element simulation. We can also obtain the free energy of the gel in different configurations. We use Eq. (6) to further take account of the effect of surface energy.

Figure 5(a) shows the normalized free energy of the gel as a function of cavity size for different chemical potentials of the solvent. For a certain range of chemical potentials of the solvent, the free energy curves show a double-well shape giving two local minima with the surface energy density $\gamma/(NkTA) = 25$. The left local minimum in the free energy landscape, as shown in the inset of Fig. 5(a), corresponds to the small cavity size, while the right local minimum corresponds to the large cavity size. We assume the system will

always stay in the configuration with the lowest free energy. When the two local free energy minima have the same value, the cavity can expand discontinuously with further decrease of the chemical potential of the solvent. The phenomenon is a reminiscent of first-order phase transition.

By selecting the cavity size which minimizes the total free energy of the gel, we plot the cavity volume as a function of the chemical potential with different surface tension densities as illustrated in Fig. 5(b). Provided a non-zero surface tension, when the chemical potential of the solvent is large, the cavity is small; when the chemical potential of the solvent is smaller than a critical value, the radius of the cavity increases discontinuously. It also shows that the critical chemical potential of the solvent is lower for a larger surface tension. When the surface tension density is zero, the growth of the cavity becomes continuous with the change of the chemical potential of the solvent, which demonstrates the importance of surface tension for the cavitation instability.

Figure 5(c) plots the shapes of the cavity and deformation of the partially constrained gel for different chemical potentials of the solvent, which correspond to the lowest free energy of the system. As discussed earlier, with the decrease of the chemical potential of the solvent, a tiny and circular cavity can dramatically expand and deform to a noncircular shape. In particular, the cavity size changes dramatically around the critical chemical potential of the solvent, which

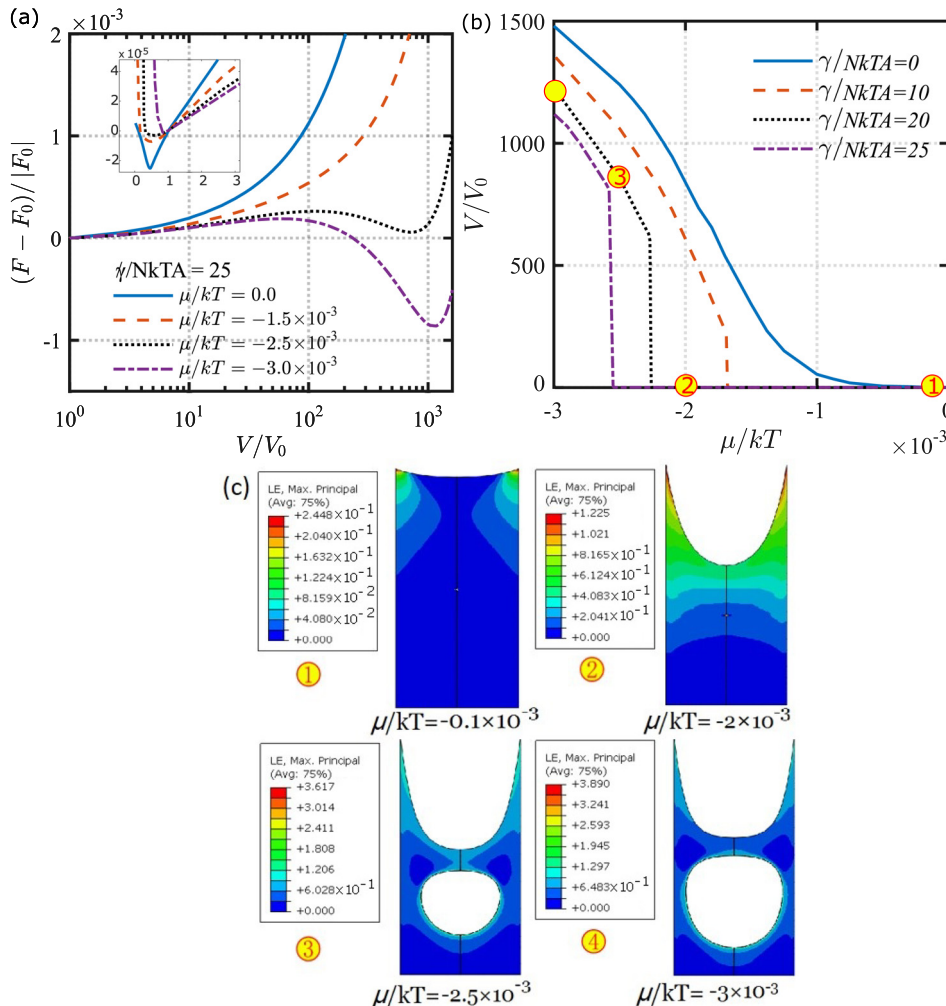


FIG. 5. (a) Free energy landscape of a partially constrained gel with a cavity (Fig. 4) as a function of the volume of the cavity, for different chemical potentials of the solvent in the environment. F_0 is the free energy of the gel when the volume of the cavity is equal to its initial value. (b) The normalized volume of the cavity as a function of chemical potential of the solvent in the environment for different surface energy densities of the gel. (c) The configurations of the gel for four different chemical potentials of the solvent in the environment with the surface energy density of the gel: $\gamma/(NkTA) = 20$. The color in the figure represents the maximal principal logarithmic strain.

may result in a discontinuous change of the reaction force exerted by the constrained walls to the gel. This is essential for the cavitation catapult mechanism as described in Sec. I.

B. Modelling of the fern cavitation catapult

A fern sporangium is typically composed of multiple cells constrained by elastic annulus walls as shown in Figs. 1(a) and 1(b). The constrained cells shrink with the decrease of the chemical potential of the solvent in the environment and actuate the bending of the elastic annulus. When the chemical potential of the solvent is decreased lower than a critical value, small cavities in the cells suddenly expand significantly causing the elastic annulus to snap back like a catapult. In this section, we will study cavitation instability in the fern sporangium.

The geometric dimensions of the fern sporangium structure are illustrated in Fig. 6(a), which are comparable to the

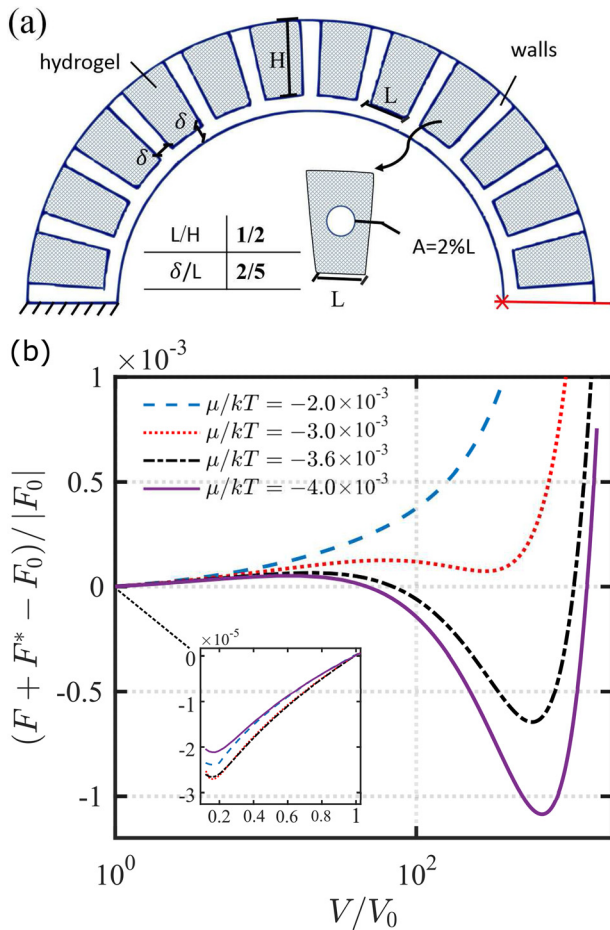


FIG. 6. (a) The schematic of a fern sporangium structure containing 12 cells and elastic walls for simulation. The right end of the structure is attached to a rigid plate to avoid end distortion. The incompressible neo-Hookean model is adopted as a material model for the elastic wall with shear modulus G . The cells are modelled by polymer gel with shear modulus given by NkT . The dimensionless parameter G/NkT represents the stiffness ratio between the elastic wall and the gel. (b) The free energy of a fern sporangium as a function of cavity volume, for four different chemical potentials of the solvent in the environment. The surface energy density of the gel, $\gamma/(NkTA)$ is set to be 20. The shear modulus ratio between the elastic wall and the gel is set to be $G/NkT = 150$. F^* is the free energy of the elastic wall, F is the free energy of the gel, and F_0 is the free energy of the entire structure when the volume of the cavity equals to its initial value.

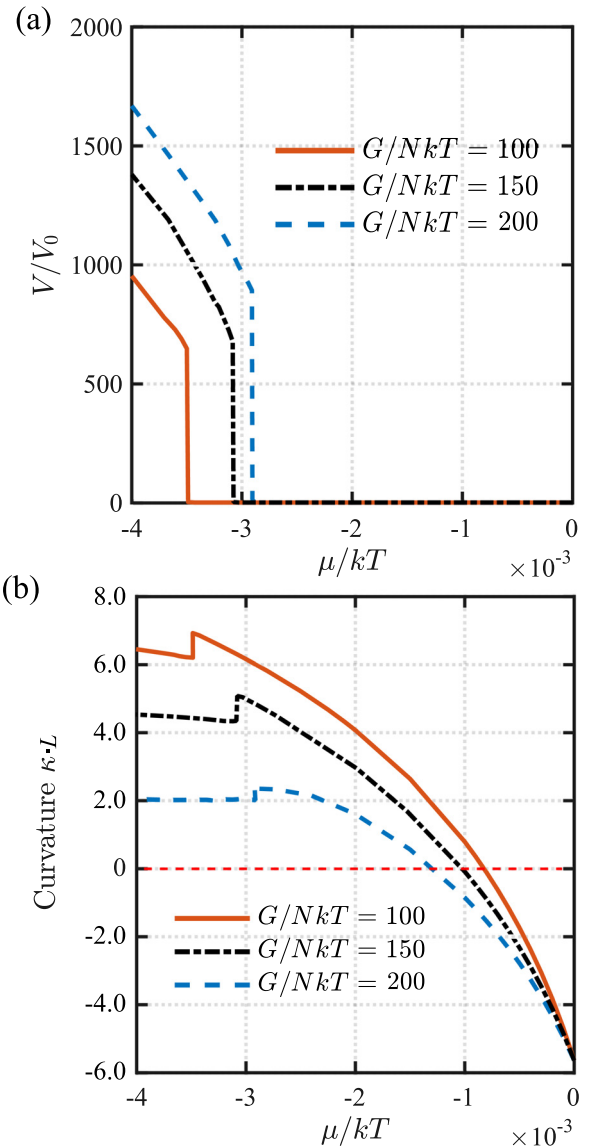


FIG. 7. The volume of the cavity and curvature change of a fern sporangium as a function of the chemical potential of the solvent in the environment. (a) The cavity expands discontinuously when the chemical potential of the solvent in the environment is decreased below a critical value. (b) The curvature of the sporangium decreases discontinuously when the chemical potential of water in the environment is below a critical value. The surface energy density of the gel is set to be $\gamma/(NkTA) = 20$.

dimensions reported in the literature.³⁰ The structure contains 12 cells with width L and height H , and the elastic annulus wall with δ denoting its thickness. 12 identical tiny cavities are introduced into the center of each cell. The initial radius of each cavity is set to be $0.02L$. The simulation procedures are similar to those in the single partially constrained gel as described above, except that the constrained walls are now elastic and deformable. To simplify the problem, we assume the deformation of all the 12 cavities is always identical. In the simulation, we use the polymer gel model summarized previously for the cells with the material parameters $N\Omega = 10^{-3}$ and $\chi = 0.2$. We adopt the incompressible Neo-Hookean model for the annulus wall with shear modulus G . Consequently, one additional dimensionless parameter G/NkT is added to the problem. The elastic modulus of the

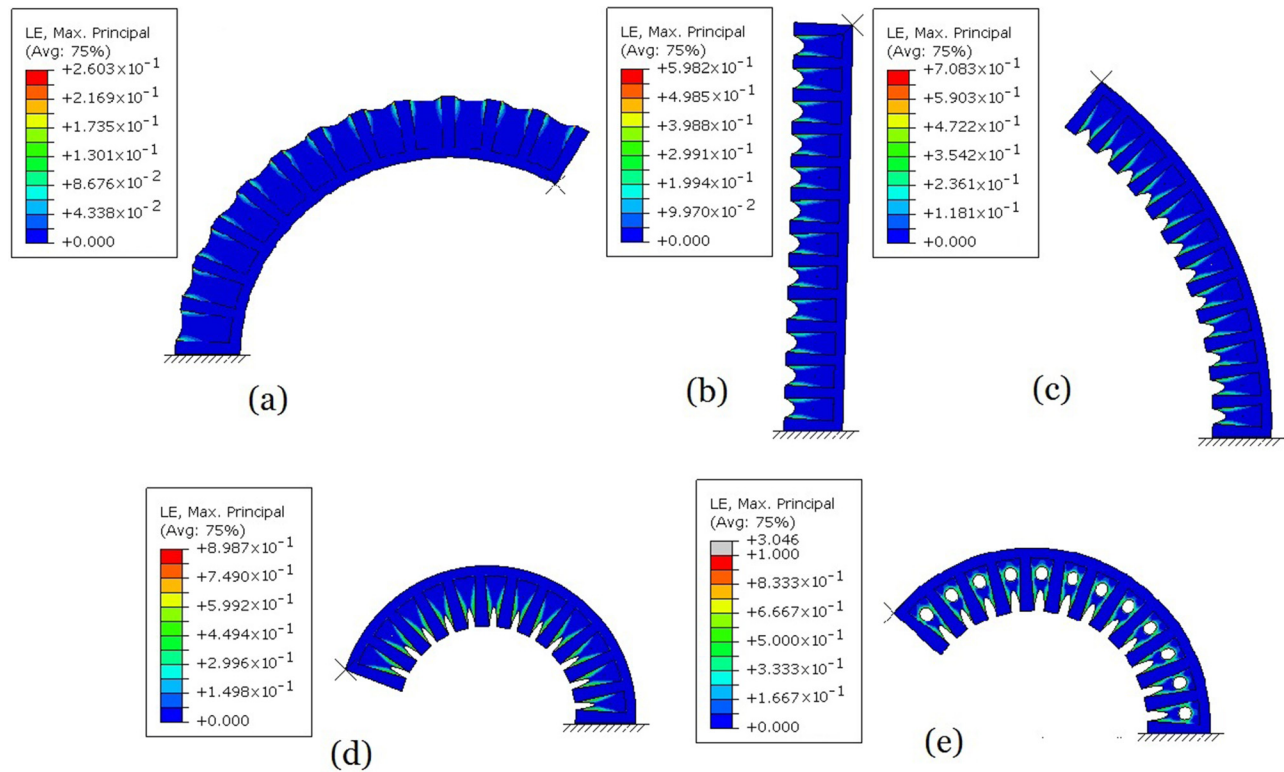


FIG. 8. The configurations of a fern sporangium with minimum free energy of the entire structure for different chemical potentials of the solvent in the environment: (a) $\mu/kT = -2.5 \times 10^{-4}$, (b) $\mu/kT = -1 \times 10^{-3}$, (c) $\mu/kT = -1.5 \times 10^{-3}$, (d) $\mu/kT = -3 \times 10^{-3}$, and (e) $\mu/kT = -3.67 \times 10^{-3}$. The surface energy density of the gel is $\gamma/(NkTA) = 20$ and the shear modulus ratio between the material of the elastic wall and the gel is set to be $G/NkT = 150$. The color in the figure represents the maximal principal logarithmic strain.

annulus wall is known to be much stiffer than the annulus cells. However, we cannot find experimental measurement of the elastic modulus of the annulus wall in the literature. Therefore, we simply assume the elastic modulus of the annulus wall is much larger than that of the annulus cell. Specifically, we set the dimensionless parameter G/NkT to be between 100 and 200.

As the chemical potential of the solvent decreases, the solvent molecules leave the gels causing shrinkage and bending of the structure. We use F and F^* to denote the free energy of the gels and elastic annulus wall, respectively. The total free energy of the structure is the summation of the two parts: $F + F^*$. Figure 6(b) shows the normalized free energy of the system as a function of the cavity volume with different chemical potentials of the solvent. Similar to Fig. 5(a), when the chemical potential of the solvent is high, the free energy curves have only one local minimum at a small cavity size; when the chemical potential of the solvent is low enough, the free energy curves show a double-well shape giving two local minima. The left local minimum in the free energy landscape corresponds to a small cavity close to its initial size. The right local minimum corresponds to the large cavity size. We also assume that the real configuration of the sporangium structure is the one which minimizes the total free energy. When the two local free energy minima have the same value, the cavities can expand discontinuously with further decrease of the chemical potential of the solvent.

Figure 7(a) shows the change of cavity volume as a function of the chemical potential of the solvent for different

stiffness of the material of the annulus wall. With decreasing stiffness of the material of the annulus wall, the critical chemical potential for the discontinuous expansion of the cavity decreases. In the system as shown in Fig. 6(a), in addition to the cavity size, the curvature of the annulus wall is also an important parameter directly relevant to the cavitation catapult mechanism. We describe the bending of the annulus wall by its curvature, defined as $\kappa = \theta/s$, where θ represents the rotating angle of the right end and s is the inner arc length of the annulus wall. The curvature is defined as a negative value when the center of curvature is on the inner side of the annulus wall. When the annulus wall deforms into a straight beam, the corresponding curvature is zero. In Fig. 7(b), we plot the curvature of the annulus wall as a function of the chemical potential of the solvent. Before the chemical potential of the solvent reaches the critical value, the curvature increases continuously with the decrease of the chemical potential of the solvent, which corresponds to the opening stage of the sporangium. The annulus is straight when the curvature is zero. When the chemical potential of the solvent reaches the critical value, the curvature of the wall drops discontinuously.

In Fig. 8, we plot the deformed configurations of the sporangium, which minimize the total free energy of the structure, with different chemical potentials of the solvent. In the plots, we set the dimensionless surface energy density $\gamma/(NkTA) = 20$ and the dimensionless shear modulus $G/NkT = 150$, corresponding to the black dash-line in Fig. 7. The order of magnitude of the dimensionless surface energy

density is determined by assuming $\gamma \sim 0.1$ N/m (the surface tension of water is around 0.07 N/m) and initial cavity size $A \sim 0.1$ μm (the size of the annulus cell is around 20 μm). When $\mu/kT=0$, the sporangium is closed in the annulus. With the decrease of the chemical potential of the solvent, the cells shrink and elastic energy is mainly stored in the annulus wall. The annulus becomes straight at $\mu/kT=-10^{-3}$, corresponding to the zero-curvature point as shown in Fig. 7(b). With further decrease of the chemical potential of the solvent, the annulus bends to the opposite direction and its curvature becomes positive. When the chemical potential of the solvent is lower than a critical value, a discontinuous expansion of cavities and decrease of curvature of the annulus wall happens. During the discontinuous reduction of the curvature, a portion of the elastic energy stored in the structure will convert to kinetic energy in a short period, which corresponds to the fast snap back of the annulus wall. We would like to point out that the predicted cavitation-induced curvature reduction as shown in Figs. 7(b) and 8 is not as big as what has been observed [Fig. 1(b)], which is probably due to two main reasons: first, our simulation is based on quasi-static assumption with completely ignoring the inertia of the structure, while the real snap back process of the sporangium is dynamic; second, the cavitation instability can induce a really large deformation in the cells and fracture may happen, which can also increase the discontinuous reduction of curvature. It is noted that certain damages in cells will not affect their functionalities and can be self-healed.

IV. CONCLUSIONS

In this article, we study the cavitation catapult mechanism in fern sporangium. In the modelling, the environmental-responsive mechanical behaviors of cells in the sporangium are described by the chemo-mechanics model of the polymer gel. Using the finite element method, we study the cavitation catapult mechanism of fern sporangium through energetic analyses. With continuous decrease of the chemical potential of the solvent, we successfully predict a sudden and discontinuous cavity expansion in the cells of fern sporangium, and also the corresponding abrupt decrease of curvature of the annulus wall. It is consistent with the recent experimental observations in fern sporangium. Through our analysis, we also found out that the magnitude of surface energy density of the cell and shear modulus of the sporangium wall play important roles in the cavitation catapult phenomenon. The results obtained and the modelling method presented in the article may be directly applicable for designing structures using responsive gels to realize the cavitation catapult mechanism.

ACKNOWLEDGMENTS

S. Cai acknowledges the support of the ONR (Grant No. N00014-17-1-2056). K. Li acknowledges the support from the Chinese Natural Science Foundation (Grant No.

11402001). C. Wang acknowledges the financial support from the National Natural Science Foundation of China, 11572099; the Natural Science Foundation of Heilongjiang Province of China, A2015002; the Fundamental Research Funds for the Central Universities, HIT.BRETHIII.201209 and HIT.MKSTISP.2016 29; and the Aeronautical Science Foundation of China, 2016ZA77001.

- ¹C. Darwin, *On the Origin of Species by Means of Natural Selection, or the Preservation of Favored Races in the Struggle for Life* (John Murray, London, 1859).
- ²Y. Abraham and R. Elbaum, *New Phytol.* **199**, 584–594 (2013).
- ³P. Fratzl and F. G. Barth, *Nature* **462**, 442–448 (2009).
- ⁴Y. Forterre, J. M. Skotheim, J. Dumais, and L. Mahadevan, *Nature* **433**, 421–425 (2005).
- ⁵Y. Forterre, *J. Exp. Bot.* **64**, 4745–4760 (2013).
- ⁶S. Aimée, V. D. W. Marleen, P. W. J. Henselmans, L. J. L. Van, D. Dimitra, and B. Paul, *PLoS One* **11**, e0158277 (2016).
- ⁷S. Kundu and A. J. Crosby, *Soft Matter* **5**, 3963–3968 (2009).
- ⁸J. A. Zimmerman, J. J. McManus, and A. J. Crosby, *Soft Matter* **6**(15), 3632–3635 (2010).
- ⁹S. M. Hashemnejad and S. Kundu, *Soft Matter* **11**, 4315–4325 (2015).
- ¹⁰K. Y. Volokh, *Biomech. Model. Mechanobiol.* **14**(5), 1071–1079 (2015).
- ¹¹Y. Y. Lin and C. Y. Hui, *Int. J. Fract.* **126**(3), 205–221 (2004).
- ¹²S. B. Hutchens, S. Fakhouri, and A. J. Crosby, *Soft Matter* **12**, 2557–2566 (2016).
- ¹³A. N. Gent and P. B. Lindley, *Proc. R. Soc. London* **249**, 195–205 (1959).
- ¹⁴A. N. Gent and B. Park, *J. Mater. Sci.* **19**, 1947–1956 (1984).
- ¹⁵A. N. Gent, *Rubber Chem. Technol.* **63**, 49–53 (1990).
- ¹⁶A. N. Gent, *Int. J. Non-Linear Mech.* **40**(2), 165–175 (2005).
- ¹⁷A. N. Gent and C. Wang, *J. Mater. Sci.* **26**(12), 3392–3395 (1991).
- ¹⁸J. B. Estrada, M. T. Scimone, H. C. Cramer, L. Mancia, E. Johnsen, and C. Franck, *Biophys. J.* **112**, 159a (2017).
- ¹⁹H. Wang and S. Cai, *J. Appl. Phys.* **117**, 154901 (2015).
- ²⁰H. Wang and S. Cai, *Soft Matter* **11**, 1058–1061 (2015).
- ²¹J. A. Zimmerman, N. Sanabria-DeLong, G. N. Tew, and A. J. Crosby, *Soft Matter* **3**(6), 763–767 (2007).
- ²²J. Cui, C. H. Lee, A. Delbos, J. J. McManus, and A. J. Crosby, *Soft Matter* **7**(17), 7827–7831 (2011).
- ²³C. Fond, *J. Polym. Sci. B* **39**(17), 2081–2096 (2001).
- ²⁴J. Zhu, T. Li, S. Cai, and Z. Suo, *J. Adhes.* **87**(5), 466–481 (2011).
- ²⁵S. Mishra, T. E. Lacy, and S. Kundu, *Int. J. Non-Linear Mech.* **98**, 23–31 (2018).
- ²⁶M. S. Chin, B. B. Freniere, S. Fakhouri, J. E. Harris, J. F. Lalikos, and A. J. Crosby, *Plast. Reconstr. Surg.* **131**(2), 303e–305e (2013).
- ²⁷K. C. Bentz, S. E. Walley, and D. A. Savin, *Soft Matter* **12**, 4991–5001 (2016).
- ²⁸L. Pavlovsky, M. Ganesan, J. G. Younger, and M. J. Solomon, *Appl. Phys. Lett.* **105**(11), 114105 (2014).
- ²⁹X. Noblin, N. O. Rojas, J. Westbrook, C. Llorens, M. Argentina, and J. Dumais, *Science* **335**, 1322 (2012).
- ³⁰C. Llorens, M. Argentina, N. Rojas, J. Westbrook, J. Dumais, and X. Noblin, *J. R. Soc. Interface* **13**, 20150930 (2016).
- ³¹R. Alexandra and B. A. Aminoff, *Muscle Nerve* **27**, 387 (2003).
- ³²G. H. Pollack, *Jpn. J. Physiol.* **51**, 649–660 (2001).
- ³³W. Hong, X. Zhao, J. Zhou, and Z. Suo, *J. Mech. Phys. Solids* **56**, 1779–1793 (2008).
- ³⁴M. K. Kang and R. Huang, *J. Appl. Mech.* **77**(6), 061004 (2010).
- ³⁵P. J. Flory and J. Rehner, *J. Chem. Phys.* **11**, 512–520 (1943).
- ³⁶*ABAQUS Analysis User's Manual V6.5* (ABAQUS, Pawtucket, RI, 2004).
- ³⁷W. Hong, Z. Liu, and Z. Suo, *Int. J. Solids Struct.* **46**, 3282–3289 (2009).
- ³⁸J. Kang, C. Wang, and S. Cai, *Soft Matter* **13**, 6372–6376 (2017).
- ³⁹D. L. Henann and K. Bertoldi, *Soft Matter* **10**(5), 709–717 (2014).
- ⁴⁰X. Xu, A. Jagota, S. Peng, D. Luo, M. Wu, and C. Y. Hui, *Langmuir* **29**(27), 8665–8674 (2013).
- ⁴¹T. Liu, R. Long, and C. Y. Hui, *Soft Matter* **10**(39), 7723–7729 (2014).